MEAN FLOWS IN ROTATING TURBULENT CONVECTIVE SHELLS

Allan Sacha Brun & Juri Toomre
JILA, University of Colorado, Boulder CO 80309-0440, USA.

ABSTRACT

We conduct numerical simulations of turbulent compressible convection within rotating spherical shells to model solar differential rotation and meridional circulation. These 3–D simulations are carried out on massively parallel computers using the Anelastic Spherical Harmonic (ASH) code. The evolution of such convection is studied in four cases which sample several paths in achieving highly turbulent flows that are able to drive a strong differential rotation from equator to pole. The resulting angular velocity Ω profiles make reasonable contact with many aspects of the solar rotation profiles inferred from helioseismic inversions of both MDI and GONG data. The substantial contrast in Ω of order 30% achieved in our simulations of turbulent convection is considerably greater than realized in previous studies.

1. MOTIVATION

A major challenge to convection theory is to explain the pronounced differential rotation with latitude exhibited both at the solar surface and throughout much of the convection zone. Helioseismology reveals a contrast of about 21% in rotation rate near the surface between equator and 60 degrees, and a contrast of 29% in going to the higher latitude of 75 degrees. Numerical simulations of solar convection in rotating spherical shells have achieved angular velocity Ω profiles that are generally in accord with such behavior, but it has been difficult to attain such Ω contrasts with latitude when studying both laminar and more turbulent flows. We discuss here a new class of simulations, building on the earlier studies of Miesch et al. (2000) and Elliott et al. (2000), that display strong differential rotation profiles and interesting meridional circulations under turbulent conditions.

2. MODELLING APPROACH

The ASH code solves the 3–D anelastic equations of motion in a rotating spherical shell geometry (Miesch et al. 2000). These equations are fully nonlinear in velocity variables and linearized in thermodynamic variables with respect to a sperically symetric mean state having a density $\bar{\rho}$, pressure $\bar{P}$, temperature $\bar{T}$ and specific entropy $\bar{S}$ and pertubations about this mean state ρ, P, T, S i.e:

$$\nabla\cdot(\bar{\rho}\mathbf{v}) = 0, \tag{1}$$

$$\bar{\rho}\left(\frac{\partial \mathbf{v}}{\partial t} + (\mathbf{v}\cdot\nabla)\mathbf{v} + 2\boldsymbol{\Omega}\times\mathbf{v}\right) = -\nabla P + \rho\mathbf{g} - \nabla\cdot\boldsymbol{\mathcal{D}} - [\nabla\bar{P} - \bar{\rho}\mathbf{g}], \tag{2}$$

$$\begin{aligned}\bar{\rho}\bar{T}\frac{\partial S}{\partial t} &= \nabla\cdot[\kappa_r\bar{\rho}c_p\nabla(\bar{T}+T) + \kappa\bar{\rho}\bar{T}\nabla(\bar{S}+S)] \\ &- \bar{\rho}\bar{T}\mathbf{v}\cdot\nabla(\bar{S}+S) + 2\bar{\rho}\nu\left[e_{ij}e_{ij} - 1/3(\nabla\cdot\mathbf{v})^2\right]\end{aligned} \tag{3}$$

where c_p is the specific heat at constant pressure, $\mathbf{v} = (v_r, v_\theta, v_\phi)$ is the local velocity in spherical geometry in the rotating frame of angular velocity $\boldsymbol{\Omega}$, $\mathbf{g}$ the gravitational acceleration, where we have neglected the contribution coming from the centrifugal forces, κ_r the thermal diffusivity related to radiative diffusion and thermal conduction and $\mathcal{D}$ the viscous stress tensor, with components

$$\mathcal{D}_{ij} = -2\bar{\rho}\nu[e_{ij} - 1/3(\nabla\cdot\mathbf{v})\delta_{ij}], \tag{4}$$

e_{ij} is the strain rate tensor. To close the set of equations, we use for equation of state

$$\frac{\rho}{\bar{\rho}} = \frac{P}{\bar{P}} - \frac{T}{\bar{T}} = \frac{P}{\gamma\bar{P}} - \frac{S}{c_p}, \tag{5}$$

with the classical perfect gas law for hydrogen and helium:

$$\bar{P} = \mathcal{R}\bar{\rho}\bar{T} \tag{6}$$

where $\mathcal{R}$ is the universal gas constant. The bracketed term in equation (2), $\nabla\bar{P} - \bar{\rho}\mathbf{g}$, vanishes initially because the mean state begins in hydrostatic balance, but as th convection becomes established, this term becomes nonzero because of the influence of what can be regarded as a turbulent pressure. The velocity and thermodynamic variables are expanded in spherical harmonics for their horizontal structure and in Chebyshev polynomials for their radial structure. This approach has the advantage that the spatial resolution is uniform everywhere on a sphere when a complete set of spherical harmonics is used up to some maximum in degree ℓ (retaining all azimuthal order m). The anelastic approximation captures the effects of density stratification without having to resolve sound waves which would severely limit the time steps.

The model is a highly simplified description of the solar convection zone: solar values are taken for the heat flux, rotation rate, mass and radius, and a perfect gas is assumed since the upper boundary of the shell lies well below the H and He ionization zone. The computational domain extends from 0.72 R to 0.96 R, where R is solar radius, thereby concentrating on the bulk of the unstable zone and here not dealing with penetration into the radiative interior. The effects of the steep entropy gradient close to the surface has been softened by introducing a subgrid scale (SGS) transport of heat to account for the unresolved motions, and enhanced eddy diffusivities are used in these large eddy simulations (LES). The typical density difference across the shell is about 25.

A succession of increasingly nonlinear flows is studied through four simulations (shown in Figure 1) that utilize decreasing viscous and thermal diffusivities to achieve complex turbulent convection influenced by rotation. The laminar case A has a Prandtl number P_r of unity; reducing the viscosity by a factor of 4 leads to the turbulent case B with P_r=1/4, or by a factor 8 leads to the more turbulent case C with P_r=1/8. Our most complex flows in case D were obtained by reducing viscosity by a factor of 8 and thermal diffusivity by a factor of 2 relative to case A, resulting in a P_r=1/4. The latter simulation utilizes spherical harmonics up to degree 340.

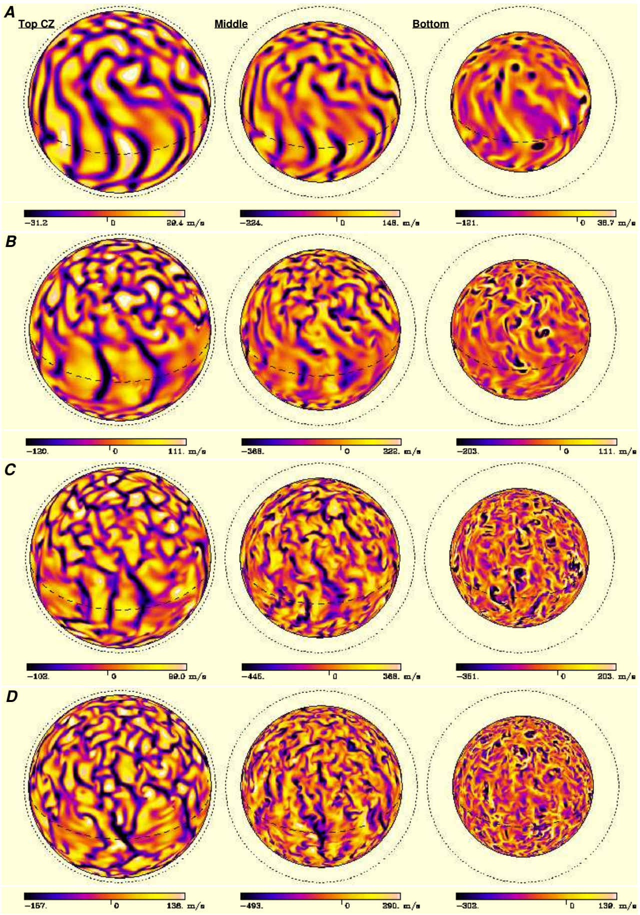

Figure 1. Convection patterns in the four cases A to D leading to increasingly turbulent flows. The radial velocity at one instant for each is shown at three depths (0.95, 0.84 & 0.73 R), with downflows in purple-dark tones and upflows in orange-bright tones. The dashed circle is positioned at radius R, and the equator is indicated.

3. RESULTING CONVECTION PATTERNS

The tendency of convection to be organized into 'banana cells' aligned with the rotation axis, as in case A in Figure 1, is progressively disrupted by increasing the level of turbulence in cases B, C and D. The convection is characterized by strong downflows whose patterns become increasingly complex, with lessened north-south alignment in the equatorial region. Many downflows extend over the full depth of the zone, as seen in comparing the patterns in the different shell cuts in Figure 1. These downflows represent 'coherent structures' that can be realized in turbulent motions with symmetries broken by rotation and stratification. These structures have a crucial role in the Reynolds stresses that serve to redistribute angular momentum and thus drive the differential rotation in such shells.

The convection is highly time dependent and complex. The evolution of the convection patterns is shown in Figure 2 for a time sequence in case D that samples one solar rotation, as viewed from a uniformly rotating frame. The downflow patterns evolve quite rapidly, and are also displaced and sheared by the associated differential rotation with latitude. Frequent cyclonic swirling features arise at the interstices of the downflow network in the turbulent cases.

4. DIFFERENTIAL ROTATION

The differential rotation that is driven by the convection is shown in Figure 3 for the four simulations. The angular velocity exhibits subtantial variations in time, and thus long time average must be formed to deduce the time mean profiles of Ω shown there. All four simulations yield Ω with a fast equator and slow polar regions.

The contour plot and radial cuts of Ω in case A possess a behavior much like the helioseismic findings: the rotation rate is nearly constant on radial lines

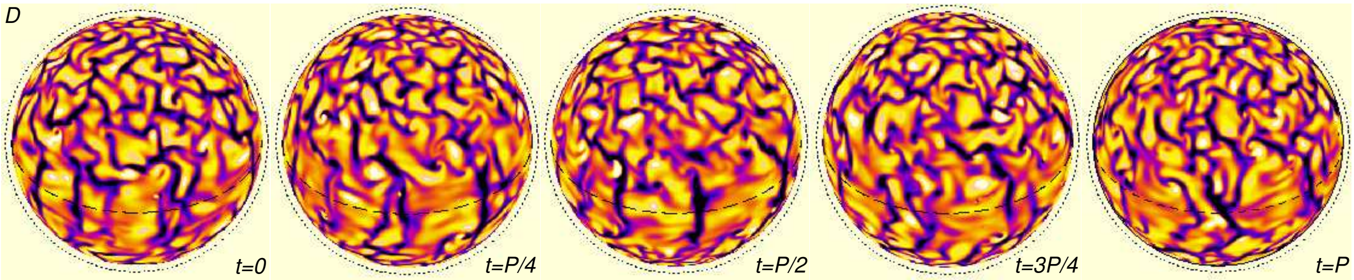

Figure 2. *Evolution of the convection over one solar rotation, showing the radial velocity of case D near the top of the domain. The time interval between each successive image is about 7 days.*

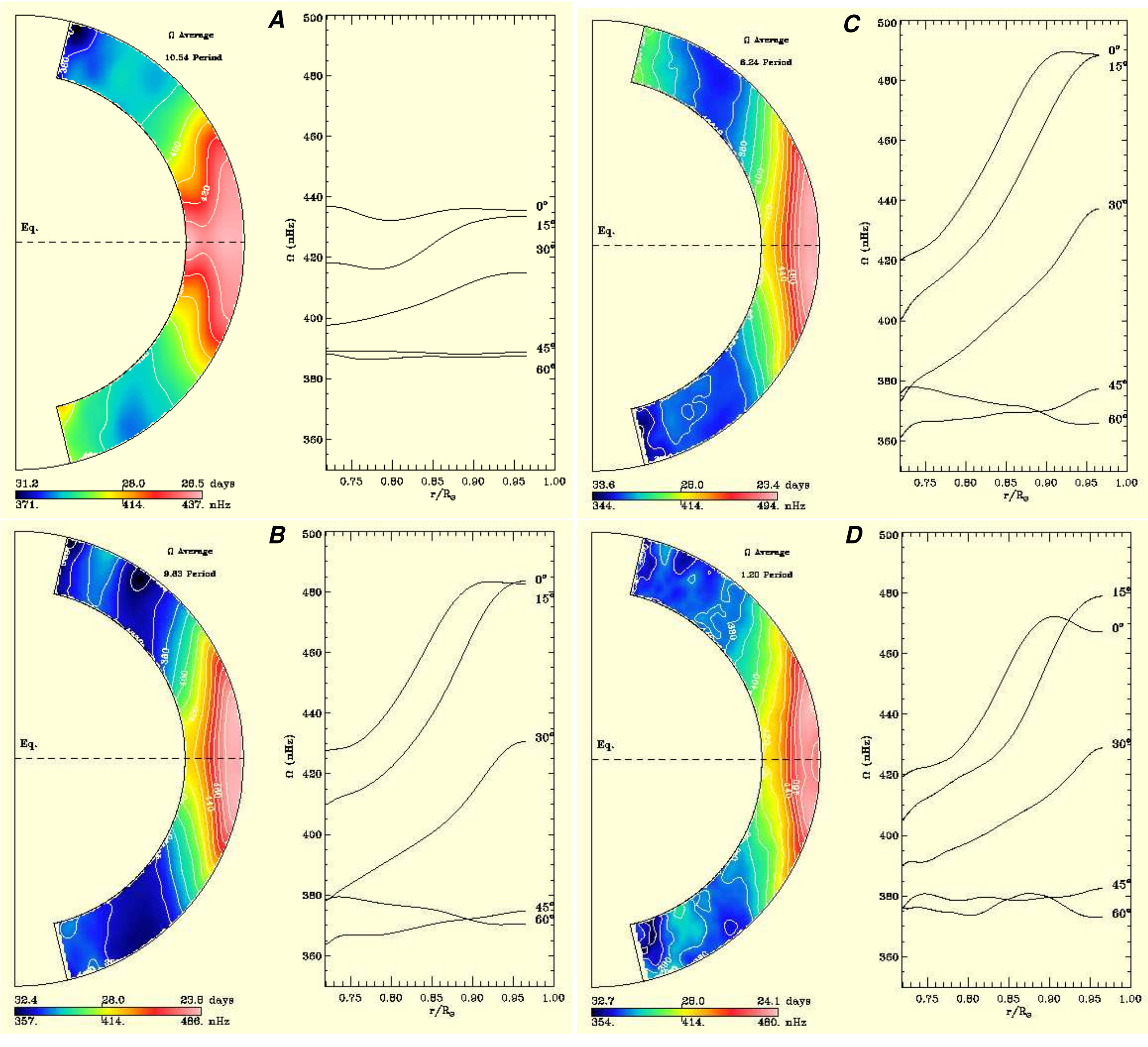

Figure 3. *Time-averaged angular velocity profiles achieved in the four simulations. The contour plots for* Ω *on the left are independently scaled, whereas the radial cuts at the indicated latitudes share the same scaling to accentuate the overall behavior of the four cases.*

and is decreasing with latitude in going from the equator to 45 degrees. However, there is little further change at yet higher latitudes, unlike in the Sun. As well, there is no tachocline of rotational transition at the base of the convection zone, for these models ignore all coupling to a radiative interior since they consider only the redistribution of angular momentum within the unstable zone. Near the top of that zone, case *A* has a contrast in angular velocity, or $\Delta\Omega$, of about 50 nHz between the equator and 60

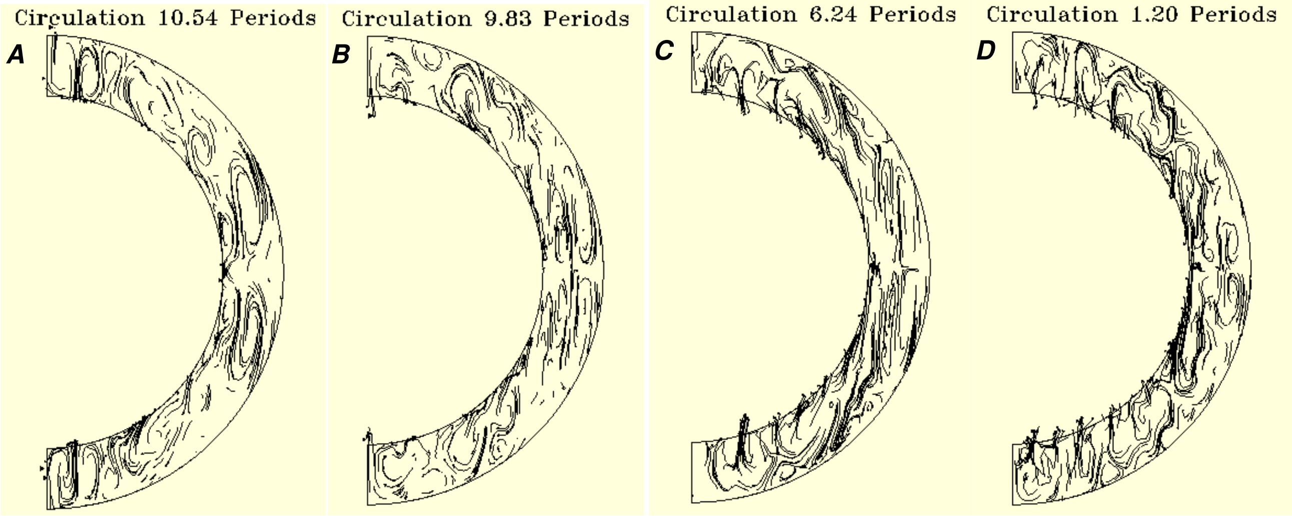

Figure 4. Time-averaged meridional circulations in the four cases. The typical speeds in these flows suggested by the trajectories with arrows are about 15 m/s.

degrees, or 12% relative to the frame rotation rate.

Turning to the more turbulent cases B and C, the contrast in angular velocity has increased subtantially, with $\Delta\Omega$ becoming 115 nHz and 125 nHz in the two cases. These correspond to a 28% and a 30% variation of the rotation rate. This is comforting since the helioseismic inferences have a contrast of about 90 nHz between the equator and 60 degrees, or a variation of about 21% in rotation rate, which further increases to 29% in going to 75 degrees. The pronounced differential rotation in cases B and C is accompanied by the Ω profiles becoming somewhat more aligned with the rotation axis, resulting in steeper slopes in the radial cuts at low and mid latitudes. These two turbulent cases achieve their larger $\Delta\Omega$ by both faster equatorial rotation rates and slower rates at higher latitudes.

Case D has somewhat more turbulent flows achieved by a different path in parameter space. The strong contrast in Ω continues to be present, with a $\Delta\Omega$ of 105 nHz or a 25% variation between the equator and 60 degrees. The variation of Ω in the radial cuts is reduced as compared to cases B and C, suggesting that such turbulent convection possessing coherent structures may provide a promising route for understanding the differential rotation achieved in the Sun. It is interesting that the increase in overall kinetic energy with increasing turbulence in our four cases is accompanied with a comparable increase in the kinetic energy of the differential rotation. The manner in which this comes about has subtleties concerning the coherent downflow structures and their contribution to the Reynolds stresses.

5. MERIDIONAL CIRCULATION

The time-averaged meridional circulation that accompanies the vigorous convection in the four cases is shown in Figure 4. The typical amplitudes in these large-scale circulations is about 15 m/s, and thus comparable to the values deduced both from time distance and ring diagram analyses. There is little change in meridional circulation amplitudes as we increase the level of turbulence from case A to D. However, multi-cell structures in these circulations become more evident with the increased complexity of the convection. At lower latitudes the circulation in both hemispheres is poleward near the top of the domain, with return flows at greater depths. Some cases display multiple cells with depth. Since the convection itself has substantial variations with time, so does the longitude-averaged meridional flow. Our deductions about the patterns of the meridional circulation may require even longer time averages than have been feasible in these simulations. It is encouraging that we have poleward circulations in the upper regions of the simulations, which is in accord with the general sense of the mean flows deduced from local helioseismology close to the surface.

REFERENCES

Elliott, Miesch & Toomre (2000), ApJ 533, 546.

Miesch, Elliott, Toomre, Clune, Glatzmaier & Gilman (2000), ApJ 532, 593.